Title

Mitochondrial growth and division during the cell cycle in HeLa cells

Journal

Journal of Cell Biology, 74(2)

ISSN

0021-9525

Authors

Posakony, JW
England, JM
Attardi, G

Publication Date

1977-08-01

DOI

10.1083/jcb.74.2.468

Peer reviewed

MITOCHONDRIAL GROWTH AND DIVISION DURING THE CELL CYCLE IN HeLa CELLS

JAMES W. POSAKONY, JAMES M. ENGLAND, and GIUSEPPE ATTARDI

From the Division of Biology, California Institute of Technology, Pasadena, California 91125. Dr. England's present address is The Wistar Institute, Philadelphia, Pennsylvania 19104.

ABSTRACT

The growth and division of mitochondria during the cell cycle was investigated by a morphometric analysis of electron micrographs of synchronized HeLa cells. The ratio of total outer membrane contour length to cytoplasmic area did not vary significantly during the cell cycle, implying a continuous growth of the mitochondrial outer membrane. The mean fraction of cytoplasmic area occupied by mitochondrial profiles was likewise found to remain constant, indicating that the increase in total mitochondrial volume per cell occurs continuously during interphase, in such a way that the mitochondrial complement occupies a constant fraction (~10–11%) of the volume of the cytoplasm. The mean area, outer membrane contour length, and axis ratio of the mitochondrial profiles also did not vary appreciably during the cell cycle; furthermore, the close similarity of the frequency distributions of these parameters for the six experimental time-points suggested a stable mitochondrial shape distribution. The constancy of both the mean mitochondrial profile area and the number of mitochondrial profiles per unit of cytoplasmic area was interpreted to indicate the continuous division of mitochondria at the level of the cell population. Furthermore, no evidence was found for the occurrence of synchronous mitochondrial growth and division within individual cells. Thus, it appears that, in HeLa cells, there is no fixed temporal relationship between the growth and division of mitochondria and the events of the cell cycle.

A number of statistical methods were developed for the purpose of making numerical estimates of certain three-dimensional cellular and mitochondrial parameters. Mean cellular and cytoplasmic volumes were calculated for the six time-points; both exhibited a nonlinear, approx. twofold increase. A comparison of the axis ratio distributions of the mitochondrial profiles with theoretical distributions expected from random sectioning of bodies of various three-dimensional shapes allowed the derivation of an "average" mitochondrial shape. This, in turn, permitted calculations to be made which expressed the two-dimensional results in three-dimensional terms. Thus, the estimated values for the number of mitochondria per unit of cytoplasmic volume and for the mean mitochondrial volume were found to remain constant during the cell cycle, while the estimated number of mitochondria per cell increased approx. twofold in an essentially continuous manner.

Investigations of the biogenesis of mitochondria in several eukaryotic systems have focused considerable attention on the relative involvement of the nuclear and mitochondrial genomes in this process (3, 6, 7, 20, 21). The evidence which has been obtained suggests that two phases can be distinguished in mitochondriogenesis (4): (*a*) the gross formation of the organelles and (*b*) their differentiation into functional sites of oxidative phosphorylation. The differentiative phase is clearly dependent upon products coded for by both nuclear and mitochondrial genes (3, 4, 21); the gross formation of mitochondrial membranes, on the other hand, seems to be entirely under nuclear control (3, 4, 21).

In previous studies from this laboratory the cell cycle dependence of the expression of the mitochondrial genome in HeLa cells has been investigated. It appears that both mitochondrial DNA replication and transcription occur predominantly, if not exclusively, in a restricted portion of the cell cycle, covering the late S and G2 phases (33, 34). The rate of mitochondrial protein synthesis, on the other hand, increases about twofold during interphase on a per cell basis, remaining fairly constant throughout the cell cycle on a per unit mass basis (12). In the present work, a morphometric analysis at the ultrastructural level has been applied to synchronized HeLa cells, to examine the relationship between the growth and division of mitochondria[1] and the events of the cell cycle.

Previous investigations of the temporal behavior of mitochondrial growth and division have centered largely on lower eukaryotes. In *Neurospora* (17), *Saccharomyces cerevisiae* (15), and *Tetrahymena* (19), the mitochondrial to cytoplasmic volume ratio was found to be essentially constant in different stages of the growth cycle, implying a continuous increase in the volume of the mitochondrial complement. The evidence obtained in the *Neurospora* (17) and *Tetrahymena* (19) studies, as well as in a study of *Schizosaccharomyces pombe* (31), was interpreted to indicate that the *division* of mitochondria, by contrast, occurs within a restricted portion of the cell cycle in these organisms. In the case of *Saccharomyces cerevisiae* (15), on the other hand, it was concluded that mitochondrial division is not tightly coupled to the cell cycle. The results of a study on Chinese hamster cells (37) did not point conclusively to either a synchronous or a continuous mode of mitochondrial growth and division.

In the present study, it has been found that the growth of the mitochondrial outer membrane occurs continuously during interphase in HeLa cells, such that the mitochondrial complement occupies a constant fraction of the volume of the cytoplasm. The results in addition point to a stable mitochondrial shape distribution and to a continuous division of mitochondria during the cell cycle. (A previous histochemical study [35] has indicated that the mitochondrial complement in the great majority of HeLa cells exists in the form of discrete organelles.) The conclusions from the two-dimensional analysis have been expressed in three-dimensional terms by making numerical estimates of various cellular and mitochondrial parameters: thus, the estimated values for the number of mitochondria per unit of cytoplasmic volume and for the mean mitochondrial volume were both found to remain constant during interphase, while the estimated number of mitochondria per cell increased approx. twofold in an essentially continuous manner.

MATERIALS AND METHODS

Conditions of Cell Culture and Synchronization

HeLa cells (strain F-315) were grown at 37°C (~22 h generation time) in roller bottles containing modified Eagle's medium (11) plus 10% calf serum. Physiologically synchronized cell populations were produced by the selective detachment of mitotic cells from their substrate (36, 44). Three separate detachments were performed, 1 h apart, the populations thus obtained containing 86.5%, 87.2%, and 87.0% mitotic cells. To avoid possible damage resulting from cold storage, the cells collected from each detachment were pelleted at room temperature (325 g_{av}, 5 min) and plated immediately on 100-mm diameter plastic dishes for electron microscopy (10^6 cells/plate), or in the center of glass cover slips placed in 35-mm diameter plastic dishes for nuclear DNA labeling and mitotic index determinations (2×10^4 cells/cover slip).

The timing of nuclear events in the cell cycle was determined separately for each detached population. The pattern of nuclear DNA synthesis was followed by counting the percentage of labeled nuclei in light micro-

[1] The physical mechanism of mitochondrial replication is not understood in detail, but the evidence from studies on *Neurospora* (23, 24, 25), *Tetrahymena* (32), and HeLa cells (41) indicates that the number of mitochondria in growing cells increases by division of preexisting organelles, and that mitochondrial membranes grow by the addition of new components to old structures.

scope autoradiographs of cover slip cultures which were exposed at various times in the cell cycle to [*methyl*-^{3}H]thymidine (49.2 mCi/μmol, 10 μCi/ml) for 30 min at 37°C, rinsed with NaCl/K/Mg buffer (0.13 M NaCl, 0.005 M KCl, 0.001 M $MgCl_2$), and fixed in acetic acid/ethanol (1:3). The autoradiographs were prepared with Kodak AR-10 stripping film with an exposure time of ~1 wk at 4°C. The time of the peak of mitotic activity at the end of the first cell cycle was determined by counting the percent of mitotic cells in cover slip cultures, stained with 1% acetic orcein, from various points in the cycle. At least 800 cells were examined in both the autoradiographs and the mitotic index preparations.

Electron Microscopy and Light Microscope Autoradiography

The cells to be used for electron microscopy and morphometric analysis were selected from the synchronous populations at 0, 3, 7, 11, 16, and 19 h after plating. The 0- and 3-h samples were derived from the third detachment, the 7-, 11-, and 16-h samples from the second, and the 19-h sample from the first. The cells were labeled with [*methyl*-^{3}H]thymidine (49.2 mCi/μmol, 10 μCi/ml) at 37°C for 30 min immediately preceding each nominal time-point, rinsed once with trypsin solution (0.05%), incubated in the same solution for 6–10 min at 37°C, and pelleted in 4 vol of modified Eagle's medium plus 10% calf serum for 10 min at 210 g_{av}. The pellet was fixed with 3% glutaraldehyde in 0.1 M Sorensen's phosphate buffer (pH 7.4) for 10 min, broken into small pieces, and fixed for an additional 1.5 h at room temperature with frequent swirling. The tissue chunks were then washed 3 times, 30 min each, with 0.1 M Sorensen's phosphate buffer, postfixed for 1 h with 1% osmium tetroxide in 0.1 M collidine buffer (pH 7.4) at room temperature, and stained en bloc with uranyl acetate in maleate buffer (pH 5.15) (13). Finally, the material was dehydrated in a graded series of ethanols followed by propylene oxide, and embedded in Epon resin.

In a given portion of a tissue block, about five gold-to-silver thin sections were cut, followed immediately by three to four thick ($^1/_2$ μm) sections (only thin sections were cut from the 0- and 3-h blocks). The sections prepared for a single time-point were taken from at least two different tissue blocks. If sections were cut from more than one portion of an individual block, the regions cut were spaced far enough apart to avoid cutting through a given cell more than once.

The thin sections were stained with lead citrate (46). The thick sections were placed on glass microscope slides, covered with Kodak AR-10 stripping film, exposed for ~2 wk at 4°C, developed, and stained with 0.05% toluidine blue for 10–12 min.

Thin sections were examined in a Philips EM201 electron microscope, operating at 60 kV. Only cell profiles containing a nuclear profile (or chromosome profile in the case of the 0-h sample) were considered for analysis. In the 7-, 11-, 16-, and 19-h samples, cell profiles in a given thin section were correlated with the profiles seen in the corresponding thick-section autoradiograph, and could thus be classified as having either labeled or unlabeled nuclei. Fig. 1*a* shows a grid square containing a region of a thin section from the 16-h point; the corresponding region of the thick-section autoradiograph is shown in Fig. 1*b*. Cells with labeled and unlabeled nuclei are clearly distinguishable. This technique provided a means of selecting a cell population for each time-point which excluded cells which were out of phase. Thus, only cells with unlabeled nuclei were photographed for the 7- and 11-h points (G1 phase), and for the 19-h point (G2 phase); similarly, only cells with labeled nuclei were photographed for the 16-h point (S phase). In a given grid square, all cell profiles containing a nuclear profile and meeting the appropriate labeling criterion were photographed. The micrographs were taken at original magnifications of × 975 and × 2240, for cell profile and mitochondrial profile measurements, respectively.

Analysis of Electron Micrographs

The electron micrographs (in the form of 35-mm negatives) were projected onto the measuring board of a Hewlett-Packard 9864A Digitizer, connected to a Hewlett-Packard 9820 Calculator (Hewlett-Packard Corp., McMinnville, Oreg.). The calculator was programmed to compute and record the following measurements: the cell and nuclear profile areas, and the areas, outer membrane contour lengths, and axis ratios[2] of the mitochondrial profiles. The final magnifications, which varied <2% from × 17,200 for measurement of cell profile parameters, and × 39,500 for measurement of mitochondrial profile parameters, were determined from a crossed-line diffraction grating replica photographed with each set of negatives.

With this apparatus, contour lengths were measured as the sum of many short (~2 mm) line segments, while areas were calculated using the trapezoid rule (45). Fig. 2*b* shows a computer-drawn plot of an actual tracing of the mitochondrial profiles in a typical micrograph field (Fig. 2*a*). The axes used in the determinations of the profile axis ratios are also shown.

Due to the fact that the cells with unlabeled nuclei in the 19-h population consist of both G1 and G2 cells, a minimum size criterion was established for this time-point in order to exclude contaminating G1 cells from the G2 cells to be analyzed. Preliminary measurements of the cytoplasmic areas of cell profiles in the 3-h (early G1) point showed no values >100 μm^2. Accordingly, of the cell profiles appearing in micrographs from the 19-h point, only those with cytoplasmic areas exceeding 100 μm^2 were analyzed.

[2] Defined as the ratio of the longest axis of the profile to the axis which perpendicularly bisects it.

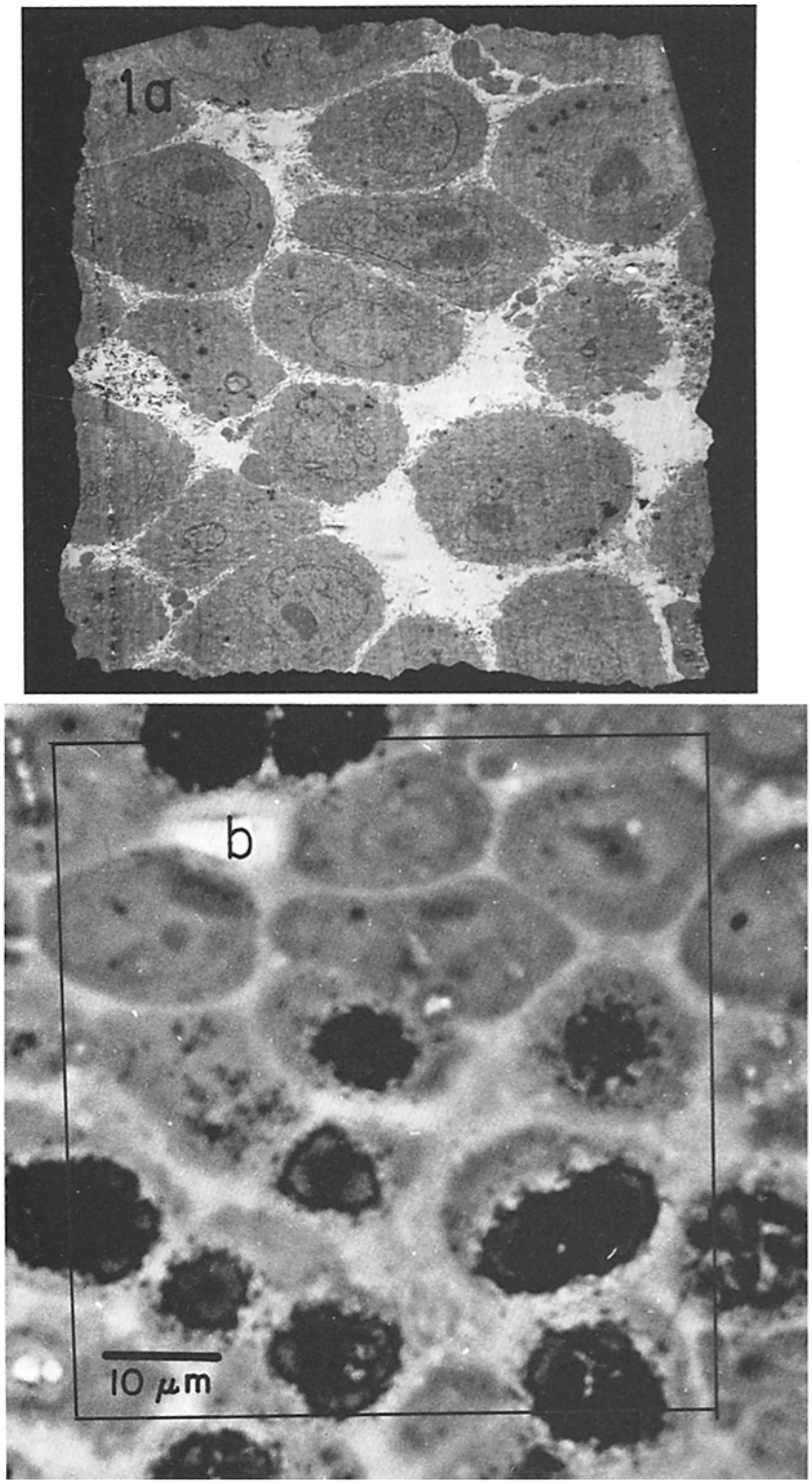

FIGURE 1 Recognition of nuclear DNA-synthesizing cells in thin sections. (*a*) Electron micrograph of a grid square containing thin-section cell profiles to be used for morphometric analysis. Cells shown are from the 16-h sample. Lead citrate stained; × 1,600. (*b*) Light micrograph of the same region (outlined in black) in an adjacent thick section subjected to autoradiography and stained with toluidine blue. Phase contrast; × 1,600. Nuclear DNA-synthesizing cells in (*a*) are readily identified by the presence of exposed silver grains over the corresponding profiles in the autoradiograph (*b*). (See Materials and Methods for details).

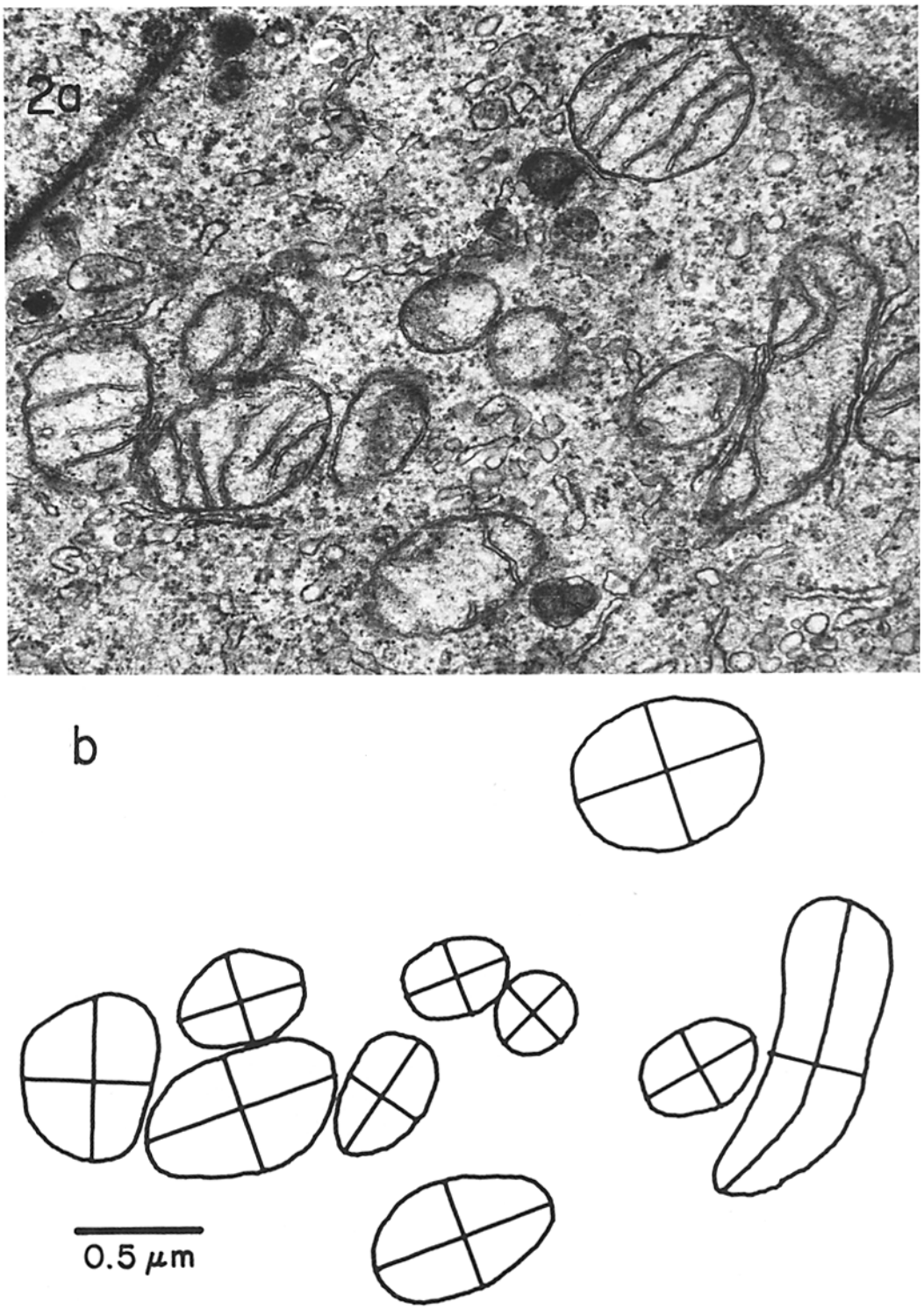

FIGURE 2 Measurement of mitochondrial profile parameters. (*a*) Electron micrograph of a typical cytoplasmic field seen in a thin section. Several mitochondrial profiles are present; portions of the nuclear profile appear in the upper corners. The magnification shown is the same as that used for tracing. Lead citrate stained; × 39,000. (*b*) Drawing of the mitochondrial profiles in (*a*) as traced using the Hewlett-Packard digitizer-calculator apparatus. Axes used in the determination of the axis ratios are also shown. (See text for details.) The drawing was prepared by a Hewlett-Packard 9862A Plotter connected to the measuring apparatus.

In the 0-h (mitotic) sample, cells which were not in a recognizable stage of mitosis (e.g., those possessing a nuclear membrane) were excluded from analysis.

For each time-point, 28–31 cell profiles were measured as described. The outer membrane contour length and area of all mitochondrial profiles in these cells (1,100–2,200 total per time-point) were measured; for ~600 mitochondrial profiles, the axis ratio was also recorded. The data were punched onto computer cards and analyzed as described below, using a Digital PDP-10 time-sharing system (Digital Equipment Corp., Maynard, Mass.) and an IBM 370/158 batch processor (IBM Corp., White Plains, N. Y.).

Derivation of Three-Dimensional Information

A number of statistical methods were developed for the purpose of estimating certain three-dimensional cellular and mitochondrial parameters from the two-dimensional data gathered in this study. These methods and their underlying assumptions are described fully in the Appendix.

Analysis of Variance

For those parameters which appeared to remain constant during the cell cycle, an F-test (8) was carried out to test the hypothesis that the mean values for the six time-points could have been obtained by random sampling from the same population. The Q values (1) reported in the Results section thus indicate the probability that the variation observed in the six mean values is due to chance and not to a real variability during the cell cycle.

RESULTS

Cell Cycle Parameters

Nuclear DNA synthesis and mitotic activity followed similar time-courses in the synchronous cultures derived from the three separate cell detachments (Fig. 3*a*). At 37°C the cell cycle was found to be ~22 h in duration (as estimated from the second peak of mitotic activity), with the maximum of nuclear DNA synthesis at 15–16 h. The culture samples taken for morphometric analysis (at 0, 3, 7, 11, 16, and 19 h after the plating of mitotic cells; see Fig. 3*a*), after cell selection by the criteria described above (Materials and Methods), provided early, middle, and late "G1" cell populations (3, 7, and 11 h), an "S" population (16 h), a "G2" population (19 h), and an "M" population (0 h).

Synchronized Cell Growth

As a measure of the growth of the synchronized cell populations, mean cellular and cytoplasmic volumes were determined (see Appendix) for each time-point. The values obtained, expressed relative to those of the 3-h sample, are shown in Fig. 3*b*. For both of these parameters, a continuous but nonlinear pattern of increase is observed, resulting in a slightly greater than twofold change over the whole cell cycle. These data and their derivation are discussed in more detail below.

Two-Dimensional Measurements

Table I and Figs. 4, 5, and 6*a–f* summarize the results obtained from electron micrographic measurements of the cellular and mitochondrial profile parameters selected for this study. The statistical treatments which were applied to these data are described in the footnotes to Table I.

Cell Profile Measurements

Columns 2, 3, and 4 of Table I show for each time-point the mean values of the cell profile areas, of the cytoplasmic profile areas[3], and of the ratios of these two parameters. A general pattern of increase in the cellular and cytoplasmic profile areas is observed from early G1 to mitosis, no doubt reflecting the growth in the average cellular and cytoplasmic volumes during the cell cycle. The mean ratio of the profile areas remains relatively constant ($Q > 0.1$).

Mitochondrial Profile Measurements

Histograms of the data on the mitochondrial profiles (area, outer membrane contour length, and axis ratio) are shown in Figs. 4, 5, and 6*a–f*. There is a striking similarity from one time-point to another both in the shapes of these distributions[4] and in their modal values. The only consistent difference appears to be a somewhat narrower distribution of the data for the 0-h point than for the other time-points. The mean values of the area, the outer membrane contour length, and the axis ratio of the mitochondrial profiles all remain essentially constant ($Q > 0.5$) during the cell cycle (Table I, columns 8, 9, and 10).

[3] (Cytoplasmic profile area) = (Cell profile area) − (Nuclear profile area).

[4] The histograms are well fitted by a log-normal distribution (39, 50) with positive skewness (J. Posakony, unpublished observations). A wide variety of physical and biological quantities exhibit frequency distributions which are more accurately described by a skewed log-normal curve than by a Gaussian (normal) curve (see reference 39).

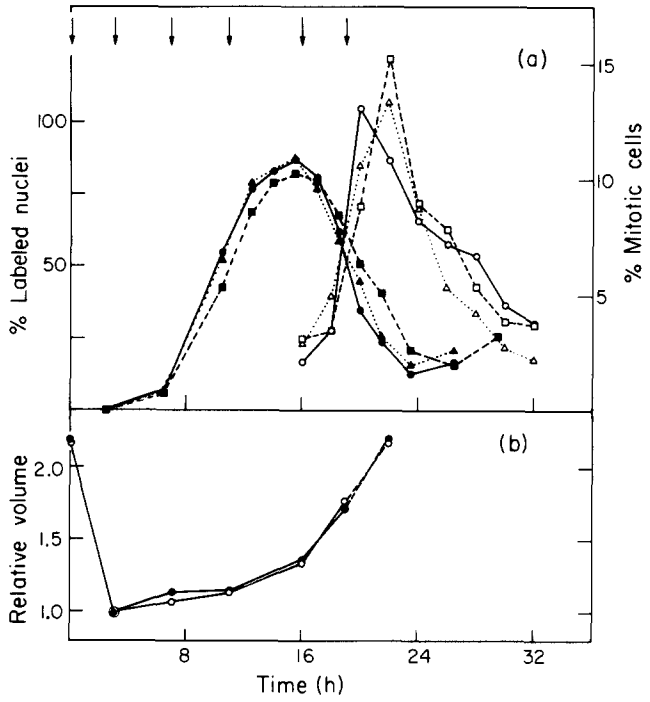

FIGURE 3 (*a*) Temporal patterns of nuclear DNA synthesis and mitosis in the synchronous cultures. The abscissa represents the time in hours after the plating of the harvested mitotic population. Solid symbols (▲, ●, ■) show the percentage of labeled nuclei observed in light microscope autoradiographs of cover slip cultures pulse-labeled with [^{3}H]thymidine at various times in the cell cycle. Open symbols (△, ○, □) represent the percent of mitotic cells observed in cover slip cultures stained with acetic orcein at various points in the cycle. Individual DNA labeling and mitotic index curves were determined for the synchronous cultures resulting from the three separate cell detachments (see Materials and Methods). The times at which culture samples were taken for morphometric analysis are indicated by the arrows at the top of the figure. (*b*) Growth of the synchronized cell population. Using the method described in the Appendix, mean cellular and cytoplasmic volumes were determined from the cell profile measurements for each time-point, and are expressed here relative to the values for the 3-h point. Closed circles represent total cell volume, while open circles represent cytoplasmic volume. The values for the 0-h point are shown twice: once at the left of the panel (0 h), and again at 22 h, where dashed lines connect them with the 19-h values. (22 h is the time of the peak of mitotic activity at the end of the cell cycle; see Fig. 3*a*.) The absolute values of these volumes (with standard errors) are given in Table II.

DATA DERIVED FROM CELL AND MITOCHONDRIAL PROFILE MEASUREMENTS

For each cell analyzed, the total area, total outer membrane contour length, and number of the mitochondrial profiles were normalized for the cytoplasmic profile area of the cell. The mean values of these ratios for each time-point are presented in Table I (columns 5, 6, and 7). Little variation ($Q > 0.5$; $Q > 0.25$; $Q > 0.25$) in these ratios is observed during the cell cycle. The ratio of total outer membrane contour length to cytoplasmic area is directly proportional to the ratio of outer membrane surface area to cytoplasmic volume (47), independent of the shape of the mitochondria. Furthermore, the ratio of total mitochondrial area to cytoplasmic area provides a reliable estimate of the corresponding volume ratio (10, 47, 49), which is also shape-independent.

Three-Dimensional Information

An attempt was made to derive from the morphometric data described above estimates of certain parameters concerning the cells and mitochondria as three-dimensional bodies (Table II). The statistical methods developed for this purpose are discussed in the Appendix.

TABLE I

*Two-Dimensional Measurements of Cellular and Mitochondrial Profiles**

(1) Time after mitosis	(2) Cell area	(3) Cyt. area‡	(4) Cyt. area / Cell area	(5) Tot. mit.¶ profile area / Cyt. area	(6) Tot. outer¶ membr. cont. length / Cyt. area	(7) no. Mit.¶ profiles / μm^2 Cyt. area	(8) Mit. profile area**	(9) Outer membrane contour length**	(10) Axis ratio**
h	μm^2	μm^2	%	%	μm^{-1}		μm^2	μm	
0	197.5 ± 9.7	133.0 ± 6.8§	67.3 ± 0.9‖	11.0 ± 0.4§	0.93 ± 0.04§	0.57 ± 0.03§	0.193 ± 0.006	1.64 ± 0.06	1.77 ± 0.11
3	117.6 ± 5.0	79.1 ± 3.3	68.4 ± 2.1	10.6 ± 0.6	0.89 ± 0.05	0.52 ± 0.03	0.202 ± 0.011	1.70 ± 0.09	1.90 ± 0.14
7	124.4 ± 7.6	78.4 ± 4.9	64.2 ± 2.0	9.4 ± 0.7	0.78 ± 0.06	0.46 ± 0.04	0.205 ± 0.016	1.69 ± 0.13	1.86 ± 0.16
11	128.9 ± 5.7	86.2 ± 4.9	66.8 ± 2.4	10.8 ± 0.7	0.90 ± 0.06	0.53 ± 0.04	0.204 ± 0.013	1.69 ± 0.11	1.84 ± 0.20
16	144.4 ± 6.1	95.1 ± 4.6	65.9 ± 1.7	10.9 ± 1.0	0.91 ± 0.08	0.54 ± 0.04	0.203 ± 0.019	1.69 ± 0.14	1.94 ± 0.20
19	170.6 ± 7.1	118.4 ± 3.5	71.3 ± 2.2	10.6 ± 0.5	0.88 ± 0.04	0.51 ± 0.03	0.210 ± 0.010	1.73 ± 0.09	1.91 ± 0.18

* Values shown are means ± standard errors, computed from the values for individual cell profiles. At each time-point, measurements were made on 28–31 cell profiles and 1,100–2,200 mitochondrial profiles.

‡ (Cytoplasmic profile area) = (Cell profile area) − (Nuclear profile area).

§ Computed from the corresponding value for the total cell area by using the estimated value of cyt. area/cell area (see following footnote).

‖ Since mitotic cell profiles lack defined nuclear and cytoplasmic regions, this value was estimated as the average of the values for the other time-points.

¶ The means and standard errors of this parameter were both computed by weighting the value of the parameter for a given cell profile according to its cytoplasmic area.

** The means and standard errors of this parameter were both computed by weighting the value of the parameter for a given cell profile according to its number of mitochondrial profiles.

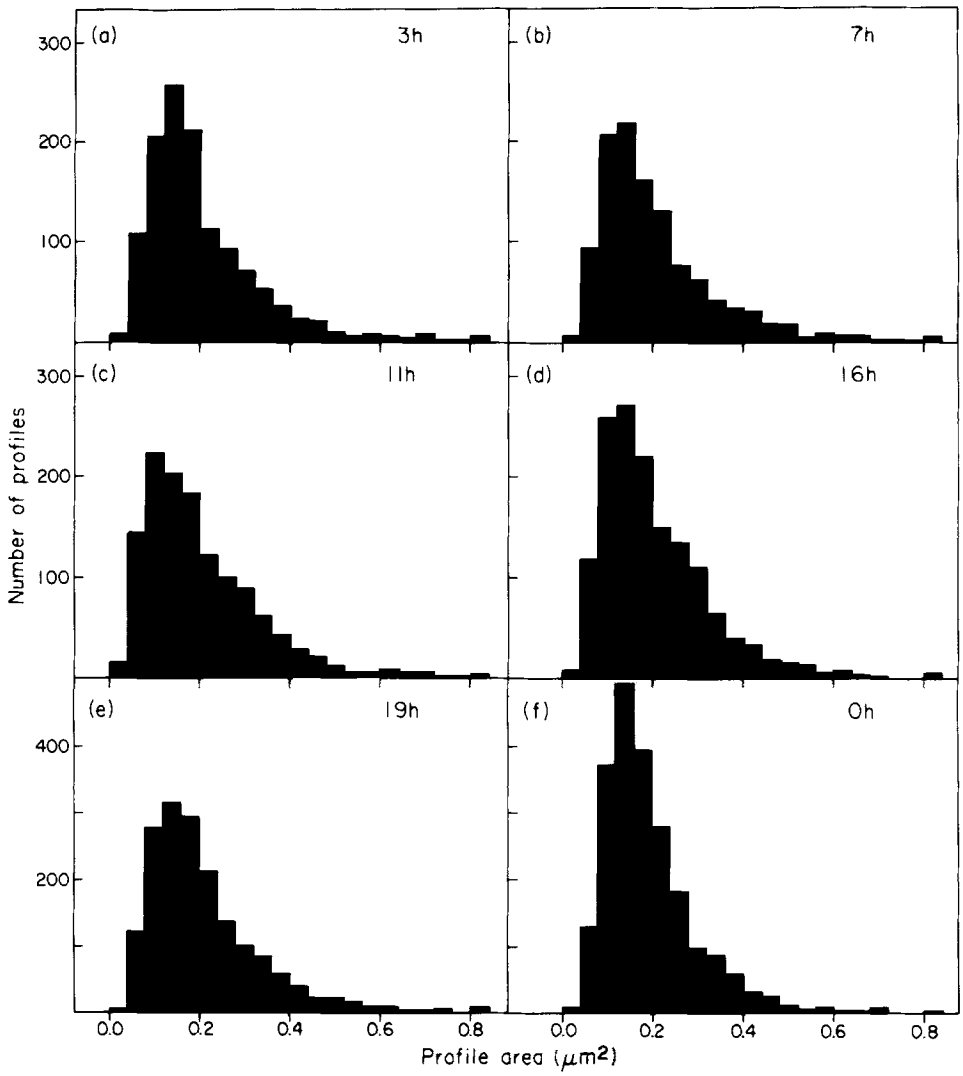

FIGURES 4-6(*a-f*) Frequency distributions of the mitochondrial profile data. In a given figure, each panel presents the distribution of the data from all cells for one time-point. These histograms were generated by a Digital PDP-10 computer, into which the raw measurements of the individual mitochondrial profiles had been read. In all three sets of histograms, the final class interval shows the total number of profiles with parameter values greater than the largest value indicated on the abscissa, i.e., profile area >0.8 μm^2, outer membrane contour length >5 μm, and axis ratio >5.

FIGURE 4 Frequency distributions, for each time-point, of the mitochondrial profiles with respect to profile area.

CELLULAR AND CYTOPLASMIC VOLUMES

The measurements of the cellular and nuclear profile areas at each time-point were used to obtain mean values of the cellular and cytoplasmic volumes. The procedure involves estimating the average ratio of the cellular and nuclear radii (assuming the cells and nuclei to be concentric spheres), and then converting the cytoplasmic area values into approximate cellular volumes (see Appendix). The equations used (reference 26 and Appendix) embody statistical corrections for: (*a*) the fact that the cell profiles analyzed were derived from cells sectioned only through their nuclei, and

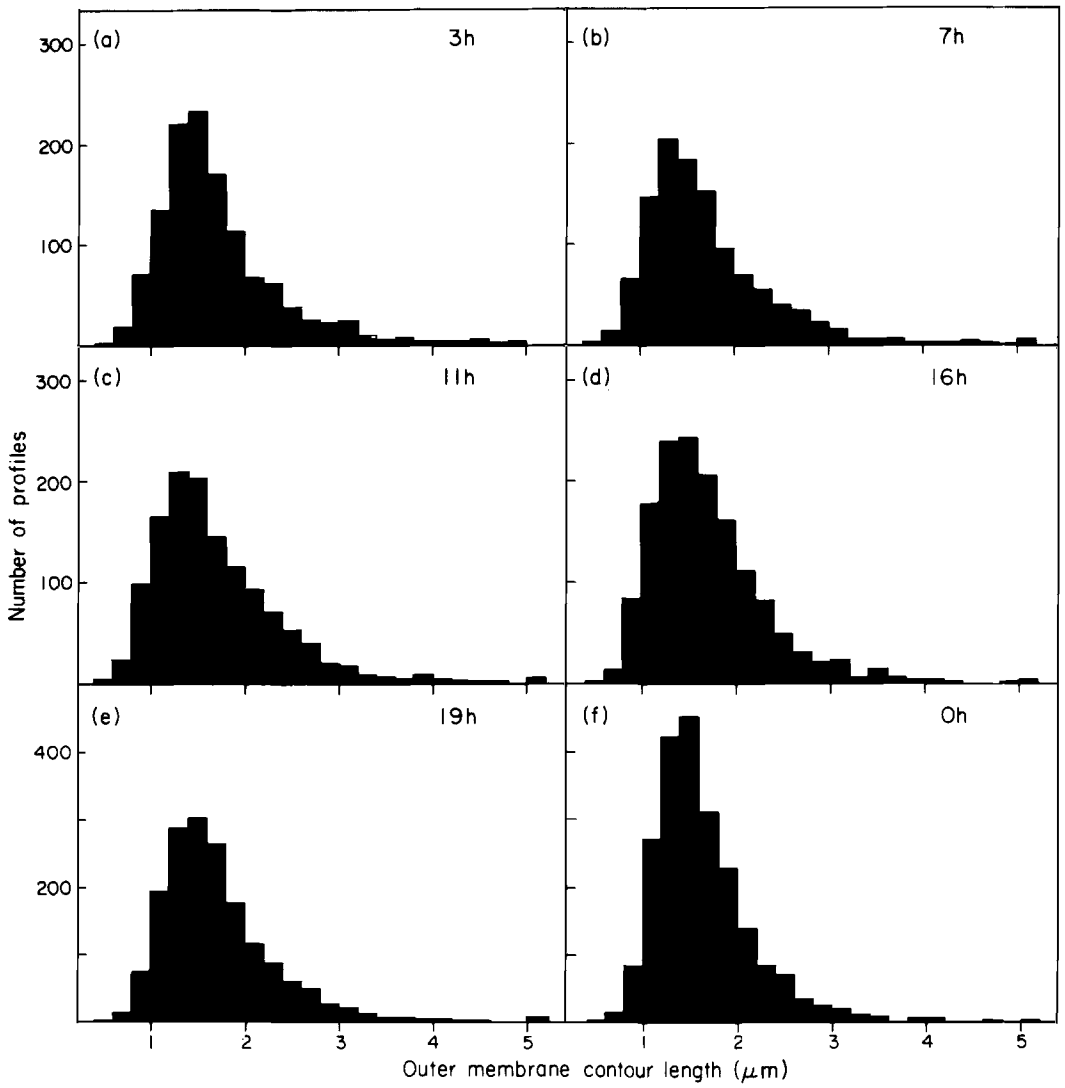

FIGURE 5 Frequency distributions, for each time-point, of the mitochondrial profiles with respect to outer membrane contour length.

(*b*) "sectioning bias", i.e., the phenomenon that a spherical nucleus is not in general sectioned through its center.

Table II (columns 2, 3, and 4) presents for each time-point the estimates of the mean cellular and cytoplasmic volumes, and their ratio, obtained by this procedure. Both volume estimates appear to increase continuously from early G1 to mitosis, exhibiting a slightly greater than twofold change over the entire cell cycle (Fig. 3*b*). The pattern of increase is not linear, but suggests an accelerating rate of growth. The ratio of the cytoplasmic and cellular volumes remains fairly constant over the cycle, indicating a proportionate increase in nuclear and cellular volumes.

THREE-DIMENSIONAL MITOCHONDRIAL PARAMETERS

OUTER MEMBRANE SURFACE AREA PER UNIT OF CYTOPLASMIC VOLUME: The mean ratios of total outer membrane contour length to cytoplasmic area (Table I) were converted to mean values of outer membrane surface area per unit of cytoplasmic volume (Table II, column 5) by multiplying by the factor $4/\pi$ (47). This conversion is independent of the shape of the

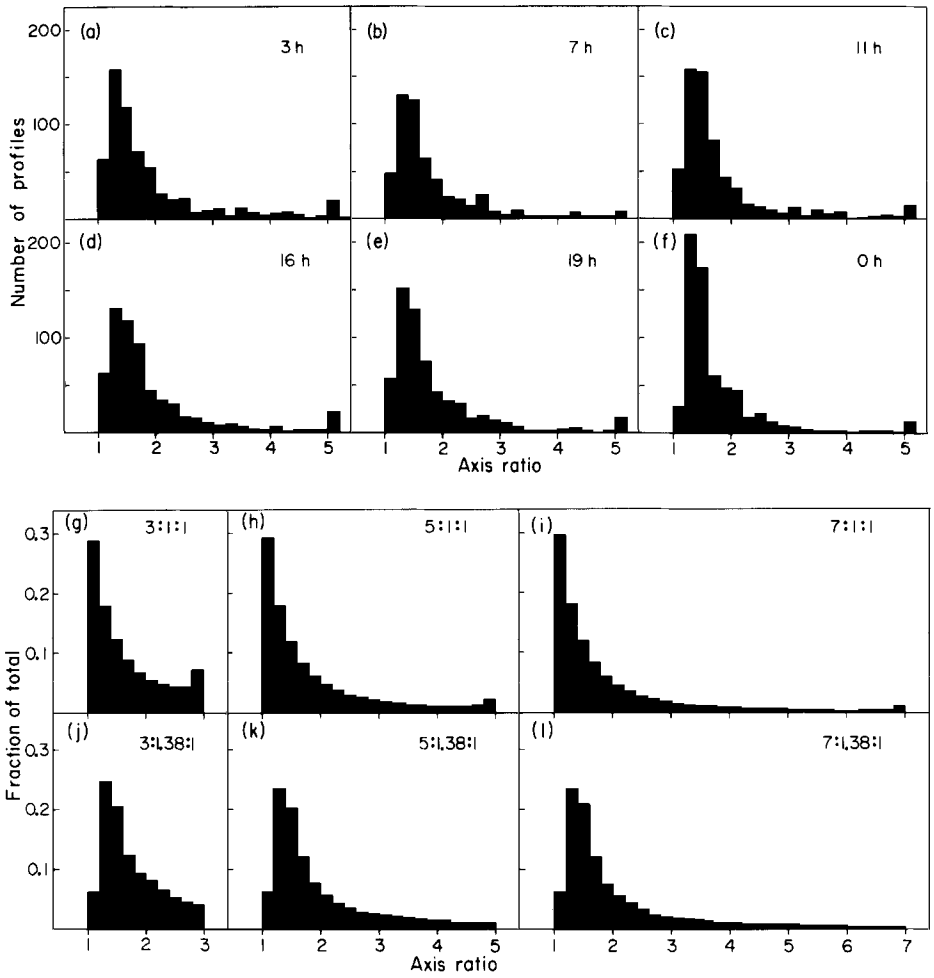

FIGURE 6(*a–f*) Frequency distributions, for each time-point, of the mitochondrial profiles with respect to axis ratio.

FIGURE 6(*g–l*) Theoretical frequency distributions of profile axis ratios, expected from random sectioning of bodies of known shapes. The upper three panels (*g–i*) show the expected profile axis ratio distributions for three prolate spheroids with different major to minor axis ratios. Class frequencies were obtained according to Equations 18 and 21 of the Appendix. The lower panels (*j–l*) show the expected profile axis ratio distributions for three general ellipsoids, all with minor axis ratio 1.38:1, and with different relative major axis length. Class frequencies were determined using the Monte Carlo method described in the Appendix, with $M = 10{,}000$. The scale of both the ordinate and the abscissa of these histograms (*g–l*) has been adjusted to make them directly comparable to the experimental frequency distributions (*a–f*).

mitochondria. That these values do not vary significantly ($Q > 0.25$) from one time-point to another implies a continuous growth of the outer membrane in terms of surface area.

MITOCHONDRIAL VOLUME FRACTION: The fraction of the cytoplasmic or cellular volume occupied by mitochondria is equivalent to the corresponding area fraction (10, 47, 49). (We have employed Formulation 2 of Mayhew and Cruz Orive [27] in applying this principle, as is appropriate for our data.) Thus, the mean values of the mitochondrial to cytoplasmic area ratios (Table I) are reproduced in column 6 of Table II. Their relative constancy ($Q > 0.5$) indicates a continuous proportionate growth of the mitochondrial and cytoplasmic volumes during the cell cycle, at

TABLE II

*Estimates of Three-Dimensional Cellular and Mitochondrial Parameters**

(1) Time after mitosis	(2) Cell vol‡	(3) Cyt. vol‡ / Cell vol	(4) Cyt. vol ¶	(5) μm^2 Outer membr.** surface area / μm^3 Cyt. vol	(6) Tot. mit. vol‡‡ / Cyt. vol	(7) no. Mit.§§ / μm^3 Cyt. vol	(8) Mit. vol¶¶	(9) no. Mit.*** / Cell
h	μm^3	%	μm^3	μm^{-1}	%		μm^3	
0	2,751 ± 211§	71.7‖	1,973 ± 151	1.19 ± 0.04	11.0 ± 0.4	0.43 ± 0.02‖‖	0.27 ± 0.01	882 ± 110
3	1,227 ± 77	72.6	891 ± 56	1.13 ± 0.06	10.6 ± 0.6	0.40 ± 0.03	0.29 ± 0.02	383 ± 48
7	1,403 ± 137	68.0	954 ± 93	0.99 ± 0.08	9.4 ± 0.7	0.35 ± 0.03	0.28 ± 0.01	389 ± 73
11	1,430 ± 121	72.1	1,032 ± 87	1.14 ± 0.08	10.8 ± 0.7	0.41 ± 0.03	0.28 ± 0.01	479 ± 76
16	1,694 ± 123	71.1	1,204 ± 87	1.16 ± 0.10	10.9 ± 1.0	0.40 ± 0.03	0.28 ± 0.01	537 ± 72
19	2,093 ± 96	74.9	1,567 ± 72	1.12 ± 0.06	10.6 ± 0.5	0.37 ± 0.03	0.31 ± 0.02	601 ± 62

* Values shown are means ± standard errors, computed from the values for individual cell profiles.

‡ Computed according to the method described in the Appendix.

§ Computed using the mean value from the other time-points of the cyt. area/cell area ratio (see Table I) and of the parameter q (Eq. 4, Appendix).

‖ Computed using the mean value from the other time-points of the parameter q (Eq. 4, Appendix).

¶ Computed for each time-point by multiplying the cell vol (column 2) by the cyt. vol/cell vol ratio (column 3).

** Computed by multiplying the values in column 6 of Table I by $4/\pi$ (47).

‡‡ Taken from column 5 of Table I.

§§ Computed using the estimator described in the Appendix (Eq. 11). A value of 3.349 was used for the shape constant (J). This is the average of the upper and lower limits for the constant, given respectively by Equations 15 and 16 (Appendix), assuming as a model shape a general ellipsoid of axis ratios 5:1.38:1 (see Results). The means and standard errors were both computed by weighting the value of the parameter for a given cell profile according to its cytoplasmic area.

‖‖ Computed using the mean value from the other time-points of the cyt. area/cell area ratio (see Table I).

¶¶ Computed for each cell by dividing the mit. vol/cyt. vol ratio by the no. mit./cyt. vol.

*** Computed for each cell by multiplying the no. mit./cyt. vol by the cyt. vol.

the level of the whole cell population. As mentioned above, this estimate of the volume fraction is independent of assumptions made about, or actual changes in, mitochondrial shape.

DERIVATION OF INFORMATION ON MITOCHONDRIAL SHAPE: A previous histochemical study in this laboratory (35) indicated that, in the great majority of HeLa F-315 cells, the mitochondrial complement is divided into distinct organelles. The work described in this and the following section was based on this finding.

Unlike the case of the volume fraction, the estimation from two-dimensional data of the number of mitochondria per unit of cytoplasmic volume requires information concerning the shape of the organelles. Accordingly, an attempt was made to obtain information about the class of organelle shapes most consistent with the mitochondrial profile measurements, and to derive a hypothetical "average mitochondrial shape" for purposes of calculation. The problem was approached by comparing the experimental frequency distributions of profile axis ratios with theoretical distributions expected from random sectioning of bodies of idealized shapes. By the use of the formulas and methods described in the Appendix, distributions were generated for three representative bodies of each of two shape classes: prolate spheroids (one long axis and two equal, shorter axes) and general ellipsoids (three axes of any length), the former being a special case of the latter. A ratio of 1.38 to 1 was chosen for the minor axis ratio of the general ellipsoids. This choice was guided initially by the modal values of the experimental axis ratio distributions (Fig. 6*a–f*), and subsequently refined by trial and error comparison of theoretical and experimental distributions. The three representative bodies of each of the two classes of shapes were given values for the longest to shortest axis ratio of 3:1, 5:1, and 7:1, the last corresponding approximately to the upper limit of the observed profile axis ratios. The theoretical distributions are presented in Fig. 6*g–l* as histograms, which are directly comparable to the histograms of the experimental axis ratios (Fig. 6*a–f*). A common feature of all the theoretical distributions is a peak occurring at the class interval which contains the ratio of the minor axes of the parent body, i.e., 1.00 for the prolate spheroids and 1.38 for the general ellipsoids. The distributions for the prolate spheroids also exhibit a significant smaller peak at the class interval containing the ratio of the major to the minor axes of the parent body, i.e., these distributions are bimodal (Fig. 6*g–l*).

A comparison of Fig. 6*a–f* and Fig. 6*g–l* reveals a close similarity in modal values, lack of bimodality (see figure legend titled "Figures 4–6[*a* to *f*]"), and overall shape between the experimental axis ratio distributions and those expected from sectioning general ellipsoids of the chosen minor axis ratio (1.38), particularly 5:1.38:1 bodies (Fig. 6*k*). Moreover, the mean value of the distribution shown in Fig. 6*k* (5:1.38:1) is 1.97, a fairly close approximation of the observed mean axis ratios (1.77–1.94 [Table I]). These similarities suggest that the observed profile axis ratio distributions, although they clearly reflect in part a variability in shape of individual mitochondria in the cell, can be closely approximated, at all stages of the cell cycle, by the axis ratio distribution expected from randomly sectioning a population of general ellipsoids with constant axis ratios of 5:1.38:1.

ESTIMATION OF MITOCHONDRIAL NUMBER DENSITY: It was shown in the previous section that the profile axis ratio distribution expected from sectioning a suitably chosen general ellipsoid, i.e., one with axis ratios of 5:1.38:1, is very similar to the experimental distributions for the mitochondrial profiles. In view of this similarity, a calculation of mitochondrial number density was made, based on an average shape for the organelles of a general ellipsoid with the above-given axis ratios. In particular, the shape constant J (see Appendix) of this ideal body was taken as an estimate of the mean shape constant used in the estimator for the number of mitochondria per unit of cytoplasmic volume (Eq. 11, Appendix).[5]

Table II shows, for each of the six time-points, the estimated number of mitochondria per unit of cytoplasmic volume, as well as values for two related parameters: the mean mitochondrial volume and the number of mitochondria per cell (columns 7, 8, and 9). While the number of mito-

[5] As discussed below (see Discussion), it has not been possible to determine precisely in our system the validity of the topological assumptions underlying this estimator; consequently, its use is to be considered tentative. Moreover, the reader is to be cautioned that there is no evidence that the 5:1.38:1 ellipsoid is the only one whose random sectioning would yield a profile axis ratio distribution fitting the experimental histogram, and furthermore, that there is no independent evidence that the shape constant of this ellipsoid is, in fact, the average shape constant for the mitochondrial population.

chondria per unit volume and the mean mitochondrial volume (as analyzed in the whole cell population) appear to be quite uniform ($Q > 0.25$; $Q > 0.5$) at the various points in the cell cycle, the number of mitochondria per cell exhibits a fairly regular increase from early G1 to mitosis, undergoing a slightly greater than twofold change throughout the cycle.[6]

Synchrony within the Individual Cell

The results presented thus far have apparently indicated that, in a population of synchronized cells, mitochondrial growth and division do not occur in a restricted portion of the cell cycle. However, the type of analysis described above would not be expected to reveal the existence of synchrony of mitochondrial growth and division within an individual cell, if the temporal relation of the mitochondrial events to the cell cycle were fixed in an individual cell, but could occur at any time in the cell cycle in different cells, with equal probability. Nonetheless, most cases of strictly intracellular synchrony should be detectable by an appropriate analysis of the data presented above. In both of the following situations, all the cells are considered to have the same mitochondrial shape distribution, independent of their stage in the cell cycle.

Assume that in each cell, both mitochondrial growth and mitochondrial division occur within intervals of time which are short compared to the total length of the cell cycle. Assume further that the relation of these events to the cell cycle, i.e., mitosis, is fixed in any individual cell, but variable among different cells. Then, at a given point in the cell cycle, a frequency distribution of cell profiles with respect to mean mitochondrial profile area should be bimodal: the relative height of the peaks corresponding to the larger and smaller mean profile area would be proportional to the average fraction of the cell cycle spent by the cells while containing "large" mitochondria relative to that spent while containing "small" mitochondria, i.e., the average fraction of the cell cycle intervening between mitochondrial growth and mitochondrial division. This would be analogous to the bimodality in nuclear DNA content observed in unsynchronized cell populations.

Now assume that mitochondrial division occurs in a short time-interval, but that mitochondrial growth occurs continuously between (mitochondrial) divisions. Assume also that the relation between mitochondrial division and mitosis is fixed in any individual cell, but is variable among different cells. Then, at a given point in the cell cycle, the frequency distribution described above should be essentially flat within the range of observed mean mitochondrial profile areas.

Fig. 7 shows, for each of the six time-points in the present study, the frequency distribution of the cell profiles with respect to mean mitochondrial profile area. These distributions exhibit a clear unimodal tendency. Thus, the present observations do not appear to contain evidence for intracellular synchrony in mitochondrial growth and division.[7]

DISCUSSION

Procedures and Sources of Error

The synchronized cell populations used for the studies reported here were prepared by the method of selective detachment of mitotic cells from their substrate (36, 44). This procedure was chosen in order to avoid any artifactual perturbation of the growth and division of mitochondria which might have resulted from the use of techniques for the induction of cell synchrony involving drug treatment or nutrient deprivation.

Due to variations in the cell cycle times of individual cells, a progressive loss of synchrony is found to occur in mitotically synchronized cell populations (28), particularly in the second part of the cycle. An autoradiographic correlation technique was employed in this study in order to recognize and exclude, from each culture sample, cells which were out of phase as judged by the criterion of nuclear DNA synthesis (see Materials and Methods and Fig. 1). After such selection, the cells actually analyzed at a given time-point were considerably more representative of a specific stage of the cell cycle than the original

[6] The greater-than-twofold change in this parameter is due to the greater-than-twofold increase observed in the mean cytoplasmic volume (Fig. 3*b*), since the estimated number of mitochondria per unit of cytoplasmic volume remains relatively constant.

[7] However, the sensitivity of this analysis is such that if, in the first situation described above, the average interval between mitochondrial growth and mitochondrial division were very short, e.g., <5% of the cell cycle, intracellular synchrony would not be detectable.

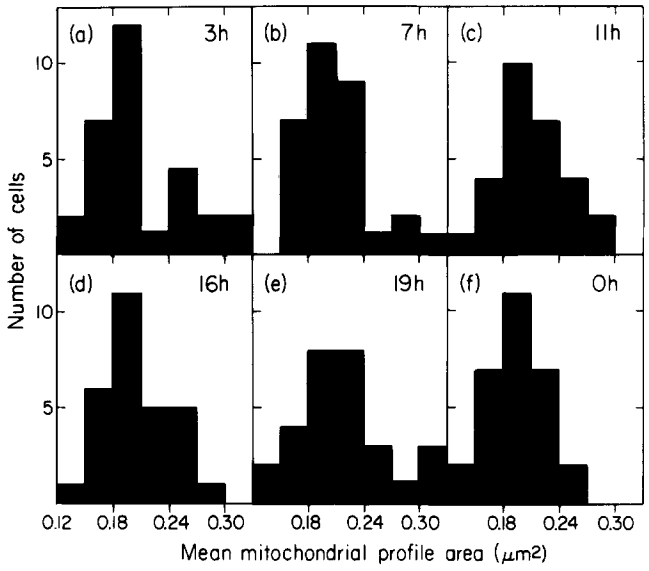

FIGURE 7 Frequency distributions, for each time-point, of cell profiles with respect to mean mitochondrial profile area.

culture sample. The use of a size criterion for cell profiles in the 19-h sample (see Materials and Methods) was similarly motivated.

The experimental approach employed here, i.e., morphometric analysis of electron micrographs of thin sections, contains a number of potential sources of error.

The effect of artifacts introduced systematically during the preparation of the cells for analysis are minimized in a study such as the present one, in which the conclusions rest largely upon relative values of experimental parameters, or upon comparison of absolute values. (The absolute numbers themselves are, of course, sensitive to such artifacts, and must be considered less reliable). Sampling errors arising from the sectioning process and from the selection of cell profiles containing nuclear profiles are also unlikely to have had a significant effect on the conclusions of this study. Accordingly, these types of errors will not be treated in detail. A possible sampling error due to the other cell selection criteria employed here is discussed in the next section.

Errors in the two-dimensional measurements may come from at least two sources. The contribution from the measuring apparatus used in this study (see Materials and Methods) is believed to be minimal. The digitizer board of this apparatus distinguishes points 0.01 inches apart; at the magnification used for measuring mitochondrial profiles, this corresponds to only 0.0064 μm. Moreover, repeated tracings of the same plane figure have yielded very similar values for both contour length and area (data not shown). The finite thickness of the tissue sections may cause an overestimation of the size of electron-opaque structures (e.g., mitochondria, outlined by membranes stained with heavy metals); this is the so-called Holmes effect (47). No correction for this effect was made in the present work, since the average "diameter" of the organelles is believed to be large compared to the thickness of the sections (see reference 47).

The numerical estimates of three-dimensional cellular and mitochondrial parameters may be in error if the assumptions underlying these estimates are not valid. The formula used here to estimate mean cellular and cytoplasmic volumes (Eq. 9, Appendix) is likely to be quite sensitive to deviations of the cells and nuclei from an assumed spherical shape or from assumed concentricity; the net result of such deviations would probably be an underestimate of the above parameters. In the evaluation of certain mitochondrial parameters (e.g., number density), the important assumption is that of convexity of the organelles (see Appendix). A light microscope examination of HeLa F-315 cells stained with diaminobenzidine (35) has indicated that the majority of mitochondria in these cells are discrete and unbranched, but true convexity in the topo-

logical sense is difficult to establish. The effect of a given deviation from organelle convexity on the values calculated for the mitochondrial parameters is not known.

Volume Growth of Synchronized HeLa Cells

The estimates made in the present study of the mean cellular and cytoplasmic volumes at various times during the cell cycle of HeLa F-315 cells indicate a continuously increasing rate of volume growth during interphase. This finding agrees well with results obtained by others in the case of HeLa S3 cells (44), Chinese hamster lung cells (40), and CHO cells (2). In the study on CHO cells (2), an exponential pattern of volume increase was observed in many of the cultures; in the others, however, the pattern was more curved, i.e., concave, than an exponential. The curve obtained in the present study (Fig. 3 *b*) is of this latter type (analysis not shown).

Due to the cell profile selection criteria applied to the 19-h (G2) and 0-h (M) samples, there is reason to believe that the mean cellular and cytoplasmic volumes determined for these time-points may be artificially high relative to those for the other time-points. In the former case, the size criterion employed in an attempt to exclude contaminating G1 cells from the sample may have also excluded profiles of small G2 cells. Similarly, in the 0-h sample, cell profile selection based on the presence of a chromosome profile may have increased the proportion of nearly equatorial sections among the cells analyzed; this phenomenon would apply especially to metaphase cells, which constituted the majority of the mitotic sample. The tendency of these effects would be to increase artificially the apparent mean cellular volumes for the respective time-points, relative to those found for the rest of interphase. Our observation of a greater than twofold increase in the mean cellular and cytoplasmic volumes during the cell cycle is quite possibly attributable to the effect just discussed regarding the 0-h sample. Nonetheless, it should be mentioned that in studies on HeLa S3 cells, under conditions where (due to loss of synchrony) one would expect to measure less than a twofold increase in mean cellular volume, Terasima and Tolmach (44) observed more than a doubling in this parameter.

The absolute values of the estimated cellular and cytoplasmic volumes (Table II, columns 2 and 4) are substantially smaller than those measured by Terasima and Tolmach (44) for the S3 strain of HeLa cells. It is not known to what degree this is due to: (*a*) differences in the methods used for estimating cellular volumes in the two studies; (*b*) an underestimation of F-315 cell volumes arising from the nonspherical shape of cells and nuclei; or (*c*) a real difference between S3 and F-315 cells.

Continuous Growth and Division of Mitochondria during the Cell Cycle

The two-dimensional data obtained here by electron micrographic measurements of various cellular and mitochondrial profile parameters provide evidence in support of a number of conclusions.

The observed constancy of the ratio of total outer membrane contour length to cytoplasmic area during the cell cycle indicates a continuous growth of the mitochondrial outer membrane in terms of surface area. This growth results in a continuous increase in total mitochondrial volume, as shown by the constancy of the mitochondrial to cytoplasmic area ratio. The volume growth occurs in such a way that the mitochondrial complement occupies a constant fraction (~10–11%) of the volume of the cytoplasm. A corollary is that the rate of mitochondrial volume growth increases continuously during interphase, in parallel with the rate of growth of cellular and cytoplasmic volumes.

The present data do not provide any information as to the behavior of the inner mitochondrial membrane during the cell cycle. However, it should be mentioned that a limited series of measurements carried out on cells from the 3-h and 19-h time-points showed no significant difference in the contour length of the inner membrane, expressed either per mitochondrial profile or per unit of cytoplasmic area.

As noted above, a previous histochemical study (35) has indicated that, in a large proportion of HeLa F-315 cells, the mitochondrial complement is divided into distinct organelles. It is therefore appropriate in this system to discuss the cell-cycle-related division of the mitochondrial mass in terms of the division of discrete bodies and to attempt to interpret the profile measurements accordingly. A prerequisite for any such interpretation of two-dimensional data is that the distribution of mitochondrial shapes at various stages of the cell cycle be known or at least be unchanged.

Though the mitochondrial population in HeLa

cells includes bodies of quite different shapes (35), the present measurements have indeed suggested that there is no appreciable change in the distribution of shapes during the cell cycle. The mean area, mean outer membrane contour length, and mean axis ratio of the mitochondrial profiles are all observed to remain essentially constant during the cycle. More importantly, the frequency distributions of these parameters are very similar from one time-point to another (with the possible exception of the 0-h point). It appears very unlikely that significant cell-cycle-dependent changes in the mitochondrial shape distribution would not be reflected in one or more of these measurements.[8]

On the basis of the foregoing considerations, the constancy of the mean mitochondrial profile area and of the number of profiles per unit of cytoplasmic area, taken together, can be interpreted to indicate a continuous division of mitochondria during the cell cycle, at the level of the whole cell population. Furthermore, no evidence has been found in this study for the occurrence of mitochondrial synchrony strictly within individual cells, though the methods of analysis available cannot rule out all models of such synchrony.

Thus, it appears that in HeLa cells there is no fixed temporal relationship between mitochondrial growth and division, on the one hand, and the events of the cell cycle, on the other. Rather, the picture that emerges is one of a steady-state process in which the mitochondrial composition of the cytoplasm remains relatively uniform during interphase.

With regard to the physical mode of mitochondrial division, no information was obtained in this study which would support unambiguously either the elongation-constriction or the transverse partition mechanism (42, 43).

As shown in a previous study from this laboratory (12), the rate of mitochondrial protein synthesis in HeLa cells increases about twofold on a per cell basis during interphase, remaining fairly constant on a per unit mass basis. The products of mitochondrial protein synthesis are essential for the functionality of the inner membrane in oxidative phosphorylation (5, 38). The finding that their synthesis occurs continuously during the cell cycle, together with the present observation of the continuous growth of mitochondria, suggests that the differentiation of these organelles into active sites of oxidative phosphorylation proceeds throughout interphase.

In contrast, both replication and transcription of mitochondrial DNA in HeLa cells occur mainly in a restricted portion of the cell cycle, covering the late S and the G2 phases (33, 34). The dissimilar temporal behavior of mitochondrial growth and mitochondrial DNA replication in HeLa cells represents a situation quite unlike that observed in bacteria, in which these two processes are closely coordinated and interdependent (18).

A constant mitochondrial to cytoplasmic volume ratio during the growth cycle has been a consistent finding in studies on mitochondrial growth and division in lower eukaryotic organisms. Mean values of ~12, 14, and 11% have been reported in *Neurospora* (17), *Saccharomyces cerevisiae* (15), and *Tetrahymena* (19), respectively, compared with ~11% in the present study. Thus, the proportionate growth of mitochondrial and cytoplasmic volumes during the cell cycle appears to be a widespread phenomenon. In the *Neurospora* (17) and *Tetrahymena* (19) studies, as well as in a study on *Schizosaccharomyces pombe* (31), morphometric data of other kinds (e.g., variations in mean mitochondrial profile area or in the number of profiles per cell section) were interpreted to indicate that the division of mitochondria occurs in a restricted part of the cell cycle in these organisms. In addition, cytological evidence of a change in mitochondrial shape during the cell cycle was obtained in these studies (17, 19, 31). On the other hand, an examination of mitochondria in *Saccharomyces cerevisiae* by serial thin sectioning led Grimes et al. (15) to conclude that mitochondrial division is not tightly coupled to the cell cycle. A study (37) in one mammalian system, Chinese hamster cells, showed parallel variations during the cell cycle in the mitochondrial to cellular profile area ratio and in the number of mitochondrial profiles per unit of cellular area. The pattern observed did not point conclusively to either a continuous or a synchronous mode of mitochondrial growth and division.

[8] However, it should be mentioned that changes in the mean relative length of the mitochondrial bodies could conceivably escape detection by the methods used here, due to the apparent insensitivity of the profile axis ratio distribution to variations in the relative length of the sectioned body above a certain value (compare, for example, Fig. 6*k* and *l*).

Numerical Evaluation of Three-Dimensional Mitochondrial Parameters

Our numerical estimates of various mitochondrial parameters (see Table II) serve to express in three-dimensional terms the interpretation given above to the two-dimensional results; namely, that the constancy of the mitochondrial to cytoplasmic volume ratio during the cell cycle represents a constancy of both of its constituent factors, the number of mitochondria per unit volume and the mean mitochondrial volume. The apparently continuous division of mitochondria is reflected in the increase in the estimated number of mitochondria per cell.

Although a specific estimate of the shape constant J was employed here for the purpose of evaluating various three-dimensional mitochondrial parameters, the relative values of these parameters at the various time-points do not depend upon the choice of a particular value of J. It suffices that the mean shape constant for the mitochondrial population (Eq. 12, Appendix) does not vary appreciably during the cell cycle. As discussed previously, no evidence has been found for a significant cell-cycle-dependent change in the mitochondrial shape distribution.

The values calculated in this study for certain mitochondrial parameters in HeLa cells can be compared with those reported by Grimes et al. (15) in their serial thin-section study on haploid and diploid strains of *Saccharomyces cerevisiae*. For the number of mitochondria per unit of cytoplasmic volume, these authors observed values of $0.85/\mu m^3$ and $1.02/\mu m^3$ (haploid and diploid strains, respectively)[9]; for the mean mitochondrial volume, the values were $0.16\ \mu m^3$ and $0.14\ \mu m^3$, respectively. The corresponding averages from the present study are $0.39/\mu m^3$ and $0.29\ \mu m^3$.

Finally, it should be mentioned that the computed values for the number of mitochondria per cell (see Table II) are quite similar to those obtained by direct count of organelles in HeLa F-315 cells stained with diaminobenzidine (J. Posakony, unpublished observations; see reference 35).

[9] The values of 850 and 1,020 per 100 μm^3 reported in the text (15) appear to be erroneous (see Table II of reference 15).

APPENDIX

ESTIMATION OF THREE-DIMENSIONAL CYTOLOGICAL PARAMETERS FROM TWO-DIMENSIONAL MEASUREMENTS MADE ON CELL SECTIONS

JOEL N. FRANKLIN. From the Department of Applied Mathematics, California Institute of Technology, Pasadena, California 91125

This appendix describes a number of statistical methods which are of use in the estimation of three-dimensional cytological parameters from two-dimensional measurements made on cell sections. The full derivations of these formulas will be published elsewhere (14). For an excellent review of stereological principles and methods, see reference 47; see also references 9, 22, 29, and 30.

Estimation of Cellular and Cytoplasmic Volumes

If one makes a random section through a sample of cells, a subpopulation of the cells is successfully cut by the sectioning plane; some of the cells in this subpopulation are cut through their nuclei. Mean cellular and cytoplasmic volumes[1] for this last group can be estimated from measurements of the cellular and nuclear profile areas, under certain assumptions concerning the shape of the cells and nuclei, their size ratio, and their relative position (see below). However, it is necessary to apply to the measurements statistical corrections which take into account (*a*) the fact that the cells under consideration were sectioned only through their nuclei and (*b*) "sectioning bias", i.e., the phenomenon that a spherical body (in this case, the nu-

[1] The cytoplasmic volume is defined as the cellular volume minus the nuclear volume.

cleus) is not in general sectioned through its center.

The method which follows[2] is based on two idealizing assumptions: (*a*) that the cells and nuclei are concentric spheres, and (*b*) that in the population under study, e.g., at a given point in the cell cycle, all cells have the same value of the parameter p, where $p = R/r$ = radius of cell/radius of nucleus; $0 \leq r \leq R$. (Note that the cells need not be of the same size.)

The first portion of the following development, leading to Equations 1–5, is a simplified version of the treatment by Mayhew and Cruz (26); Eq. 5 is the same as Correction 12 of reference 26. The development is furthermore based on the appropriateness of Formulation 2 of Mayhew and Cruz Orive (27) in the analysis of our data.

Suppose that a spherical cell (radius R) is randomly sectioned through its nucleus (radius r). The area of the resulting nuclear profile has the expected value:

$$E(A_n) = \frac{2}{3}\pi r^2; \tag{1}$$

the area of the resulting cell profile has the expected value:

$$E(A_c) = \pi R^2 (1 - \frac{1}{3p^2}). \tag{2}$$

Now consider the sectioning (through the nuclei) of a sample of cells with $R = R_1, R_2, \ldots,$ and $r = r_1, r_2, \ldots,$ in which $\frac{R_i}{r_i} = p$. The ratio of the sum of the nuclear profile areas to the sum of the cell profile areas can be expressed using equations 1 and 2. It is:

$$\frac{E(\Sigma A_n)}{E(\Sigma A_c)} = \frac{2}{3p^2 - 1}. \tag{3}$$

An experimental value, q, of this ratio can be computed from measurements of nuclear and cellular profile areas in cell sections:

$$q = \sum_{i=1}^{N} (A_n)_i \Big/ \sum_{i=1}^{N} (A_c)_i, \tag{4}$$

where N is the number of cell (or nuclear) profiles. Substituting q for the left-hand side of Eq. 3 and solving for p, we find

$$p = ([(2/q) + 1]/3)^{\frac{1}{2}}. \tag{5}$$

Given this estimate of p, the average cytoplasmic to cellular volume ratio for the cells analyzed can be calculated; it is $[1 - (1/p^3)]$. Finally, the mean cell volume of the sectioned population can be computed as follows: In each cell, the sectioning plane passes at a distance x from the common center of the nucleus and the cell. (Note that $0 \leq x \leq i$.) The resulting nuclear and cellular profile areas are, respectively,

$$A_n = \pi(r^2 - x^2) \tag{6}$$

and

$$A_c = \pi(R^2 - x^2). \tag{7}$$

The cytoplasmic profile area is:

$$A_c - A_n = \pi(R^2 - r^2) = \pi R^2 (1 - \frac{1}{p^2}), \tag{8}$$

i.e., it is independent of x. Using Eq. 8, the volume of an individual cell can be found:

$$(V_c)_i = \frac{4}{3}\pi R_i^3 = (4/3\sqrt{\pi}) \cdot [p^2/(p^2 - 1)]^{3/2} \cdot [(A_c)_i - (A_n)_i]^{3/2}. \tag{9}$$

The mean cell volume of the sectioned population is then:

$$\bar{V}_c = N^{-1} \cdot \sum_{i=1}^{N} (V_c)_i, \tag{10}$$

where N is the number of cell profiles analyzed.

Estimation of Number Density of Organelles

This section is concerned with counting the number N_V of organelles in a unit cellular or cytoplasmic volume. We wish to estimate this parameter from two-dimensional measurements made on cell and organelle profiles in random sections. Currently used estimators for N_V depend on a prior knowledge of the *sizes* of the organelles as three-dimensional bodies, e.g., the estimator of Weibel (47) and Weibel and Gomez (48) contains a coefficient K relating to the organelle size distribution. An estimator for N_V will be described (Eq. 11) which does not require information concerning the size distribution of the intact organelles.

The estimation of N_V from cross-sectional measurements rests on the assumption that the organelles under study are convex bodies. The most

[2] Another, possibly more reliable, method for estimating cellular and cytoplasmic volumes is given in reference 47.

important implication of this term is that an individual organelle yields a single profile when sectioned by a given plane; conversely, a given profile derives exclusively from the sectioning of one organelle. (Thus, it is apparent that branched or curved organelles are nonconvex bodies.) Clearly, it is important to determine the validity of the assumption of convexity in the system being investigated (see Discussion for evidence on this point in the case of HeLa cells).

If a_i represents the area of an individual organelle profile, the number of organelles per unit volume is estimated as follows:

$$N_V = J^{-1} \cdot \sum_{i=1}^{M} a_i^{-\frac{1}{2}} \cdot A^{-1}. \quad (11)$$

In this equation, M is the number of organelle profiles and A is the total cellular or cytoplasmic profile area in which the M organelle profiles were observed (depending on whether N_V is being estimated with respect to cellular or cytoplasmic volume). The number J can be called the shape constant. Each (convex) body of a given shape has a corresponding value of J, which is independent of the size of the body, e.g., $J = \pi^{\frac{1}{2}}$ for spheres of all sizes.

The estimator given in Eq. 11 remains valid even if the organelles do not all have the same shape (or shape constant). In this case, a mean shape constant is used. Suppose the organelle population contains bodies of N different shapes, with corresponding values of J: $J_1, J_2, \ldots, J_N$. Let f_i be the fraction of the population with shape i and shape constant J_i (a graph of J vs. f would describe a shape distribution for the population). The mean shape constant is then:

$$J = \sum_{i=1}^{N} (f_i \cdot J_i). \quad (12)$$

An equation will now be given (Eq. 14) defining J explicitly for the general ellipsoid. Let the ellipsoid have the semi-axes $a_1 \leq a_2 \leq a_3$. (Since J is independent of size, it depends on only two of the axis ratios of the body, say a_3/a_1 and a_2/a_1.) Suppose that the ellipsoid is centered at the origin and that its axes are oriented along the principal coordinate axes. Let $\boldsymbol{u} = (u_1, u_2, u_3)$ be any unit vector. Define the dimensionless quantity

$$I(\boldsymbol{u}) = \pi^{\frac{1}{2}}(a_1a_2a_3)^{-\frac{1}{2}} \cdot (a_1^2u_1^2 + a_2^2u_2^2 + a_3^2u_3^2)^{3/4}. \quad (13)$$

The shape constant J is the average of $I(\boldsymbol{u})$ over the unit sphere, defined by all possible $\boldsymbol{u}$ with a given origin. Taking $u_1 = \cos\phi \sin\theta$, $u_2 = \sin\phi \sin\theta$, and $u_3 = \cos\theta$,

$$J = (2/\pi) \int_o^{\pi/2} \int_o^{\pi/2} I(\boldsymbol{u}) \sin\theta \, d\theta d\phi. \quad (14)$$

The definitions of $I(\boldsymbol{u})$ and of J apply specifically to the estimator given in Eq. 11. Though the integral in Eq. 14 cannot be evaluated analytically, it can be evaluated numerically by the use of the trapezoid rule (45), Simpson's rule (45), or a Monte Carlo method (16). When only an approximate value for J is sought, the following inequalities can be employed:

$$J \leq \pi^{\frac{1}{2}} (a_1a_2a_3)^{-\frac{1}{2}} \cdot [(1/3) (a_1^2 + a_2^2 + a_3^2)]^{3/4} \quad (15)$$

$$J \geq \pi^{\frac{1}{2}} (a_1a_2a_3)^{-\frac{1}{2}} \cdot (1/3)(a_1^{3/2} + a_2^{3/2} + a_3^{3/2}). \quad (16)$$

Profile Axis Ratio Distributions

One approach toward deriving information about the three-dimensional shape of organelles is to compare experimental measurements of a given organelle profile parameter in random sections of the organelles with theoretical predictions concerning the behavior of the parameter when a body of known shape is randomly sectioned. In this section, methods are discussed for obtaining the frequency distribution of profile axis ratios expected from the sectioning of ellipsoids.

The calculus of probabilities employs two types of functions in the treatment of a random variable $t \geq 1$. One is the probability density function, denoted $p(t)$, and the other is the distribution function, $P(z)$. The relationship between the two is as follows:

$$P(z) = \text{Probability } (t \leq z) = \int_1^z p(t) \, dt. \quad (17)$$

In the present case, $P(z)$ is the probability that, when an ellipsoid is sectioned by a random plane, the profile axis ratio t is less than or equal to some chosen z.

A prolate spheroid is an ellipsoid of revolution with one long axis and two equal, shorter axes. Suppose a prolate spheroid is cut by a random plane. The resulting profile is an ellipse; it has some axis ratio $t \geq 1$. Let the spheroid have semi-axes $a_1 = a_2 < a_3$ and let $T = a_3/a_1$, i.e., T is the ratio of the long to the short axes of the spheroid.

If a section is cut normal to the long axis, the resulting profile is a circle and $t = 1$; if it is cut parallel to the long axis, $t = T$. It can be demonstrated that

$$p(t) = k \cdot t^{-3} (T^2 - t^2)^{-\frac{1}{2}} \qquad (1 \leq t \leq T). \quad (18)$$

Since we require $P(T) = \int_1^T p(t)\, dt = 1$, Eq. 18 implies:

$$k = \left[\int_1^T t^{-3} (T^2 - t^2)^{-\frac{1}{2}}\, dt \right]^{-1}, \quad (19)$$

or

$$k = [(T^2 - 1)^{\frac{1}{2}} (2T^2)^{-1} + (2T^3)^{-1} \cdot \ln [T + (T^2 - 1)^{\frac{1}{2}}]]^{-1}. \quad (20)$$

The construction of a frequency distribution (histogram) of t from Eq. 18 is discussed below (Eqs. 21 and 22).

In the present study, we were interested in computing profile axis ratio distributions for general ellipsoids (of which prolate spheroids are a subset). For this general case, a method will now be described which involves a Monte Carlo (numerical) (16) calculation of the distribution function $P(z)$, rather than an explicit formula for the probability density $p(t)$ (such as given above in Eq. 18 for prolate spheroids).

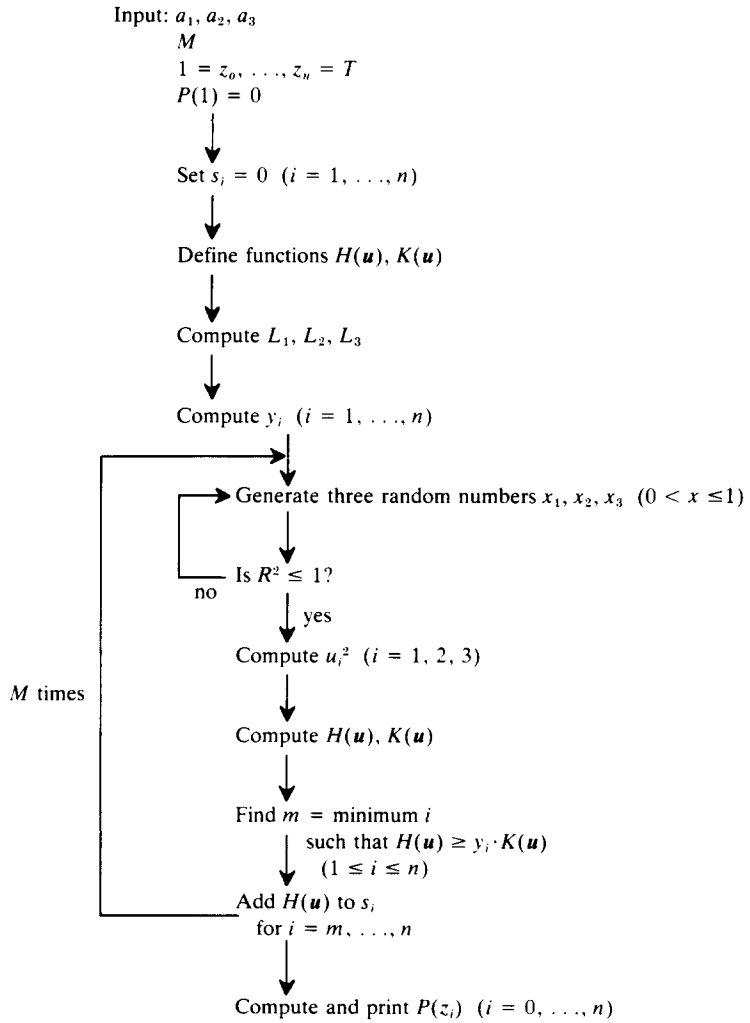

FIGURE A 1 Flow-chart diagram of the Monte Carlo method for computing profile axis ratio distributions for general ellipsoids. The input information is explained in the text; equations for the other functions are given in Table A-I.

Let the ellipsoid have semi-axes $a_1 \leq a_2 \leq a_3$ and $T = a_3/a_1$, i.e., T is the ratio of the longest to the shortest axis. The Monte Carlo approach to the calculation of $P(z)$ is summarized in Table A-I and Fig. A 1. The parameter M is the desired number of iterations in the calculation; the error in the method is of the order $1/\sqrt{M}$. The computing machine is given the values of a_1, a_2, a_3; M; and $P(1) = 0$. For the purposes of constructing a frequency distribution of t (see below), $P(z)$ is calculated at an appropriate number n of values of z (generally equally spaced) in the interval $1 \leq z \leq T$. Thus, the computer is also given the desired z's, with $z_0 = 1$ and $z_n = T$. It is then programmed to carry out the Monte Carlo calculation, as shown in Fig. A 1, using the equations in Table A-I.

The frequency distribution of the parameter t may be represented by a histogram (see Fig. 6*g–l*). The frequency f_i corresponding to a given interval I_i is computed from $p(t)$ or $P(z)$ as follows:

$$f_i = \int_{z_{i-1}}^{z_i} p(t)\, dt, \tag{21}$$

or

$$f_i = P(z_i) - P(z_{i-1}), \tag{22}$$

so that I_i is the interval from z_{i-1} to z_i. The two equations are equivalent, since,

$$f_i = \int_{z_{i-1}}^{z_i} p(t)\, dt = \int_1^{z_i} p(t)\, dt - \int_1^{z_{i-1}} p(t)\, dt = P(z_i) - P(z_{i-1}). \tag{23}$$

A comparison has been made between the f_i's obtained from Eq. 18 and those given by the Monte Carlo method (M = 10,000), when both are applied to a prolate spheroid of axis ratios 3:1:1 (J. Posakony, unpublished observations). The values are in complete agreement within the error of the Monte Carlo calculation.

TABLE A-I

Equations Used in the Monte Carlo Method for Computing Profile Axis Ratio Distribution for General Ellipsoids*

$L_1 = 1/a_1^2$
$L_2 = 1/a_2^2$
$L_3 = 1/a_3^2$
$y_i = [(z_i + z_i^{-1})\sqrt{L_1L_2L_3}]^{-1} \quad (i = 1, \ldots, n)$
$R^2 = x_1^2 + x_2^2 + x_3^2$
$u_1^2 = x_1^2/R^2$
$u_2^2 = x_2^2/R^2$
$u_3^2 = x_3^2/R^2$
$H(\boldsymbol{u}) = (u_1^2/L_1 + u_2^2/L_2 + u_3^2/L_3)^{1/2}$
$K(\boldsymbol{u}) = u_1^2(L_2 + L_3) + u_2^2(L_1 + L_3) + u_3^2(L_1 + L_2)$
$P(z_i) = s_i/s_n \quad (i = 1, \ldots, n);\ P(z_0) = P(1) = 0$

* See Fig. A 1.

The generosity of Dr. Jerome Vinograd and Dr. Norman Davidson in making available their digitizer-calculator apparatus is gratefully acknowledged.

This work was supported by National Institutes of Health grant GM-11726, a Dernham Fellowship (D196) of the American Cancer Society to J. England, and a National Science Foundation Summer Research Traineeship to J. Posakony.

Received for publication 29 April 1976, and in revised form 12 April 1977.

REFERENCES

1. ABRAMOWITZ, M., and I. A. STEGUN, editors. 1964. *Handbook of Mathematical Functions*. Dover Publications, Inc., New York.
2. ANDERSON, E. C., G. I. BELL, D. F. PETERSEN, and R. A. TOBEY. 1969. Cell growth and division. IV. Determination of volume growth rate and division probability. *Biophys. J.* **9**:246–263.
3. ASHWELL, M., and T. S. WORK. 1970. The biogenesis of mitochondria. *Annu. Rev. Biochem.* **39**:251–290.
4. ATTARDI, G., P. COSTANTINO, J. ENGLAND, D. LYNCH, W. MURPHY, D. OJALA, J. POSAKONY, and B. STORRIE. 1975. The biogenesis of mitochondria in HeLa cells: a molecular and cellular study. In *Genetics and Biogenesis of Mitochondria and Chloroplasts*, C. W. Birky, Jr., P. S. Perlman, and T. J. Byers, editors. The Ohio State University Press, Columbus, Ohio. 3-65.
5. BEATTIE, D. S. 1971. The synthesis of mitochondrial proteins. *Sub-cell. Biochem.* **1**:1–23.
6. BIRKY, C. W., JR., P. S. PERLMAN, and T. J. BYERS, editors. 1975. *Genetics and Biogenesis of Mitochondria and Chloroplasts*. The Ohio State University Press, Columbus, Ohio.
7. BOARDMAN, N. K., A. W. LINNANE, and R. M. SMILLIE, editors. 1971. *Autonomy and Biogenesis of Mitochondria and Chloroplasts*. North-Holland Publishing Co., Amsterdam.
8. CROXTON, F. E. 1953. *Elementary Statistics with Applications in Medicine and the Biological Sciences*. Dover Publications, Inc., New York.
9. CRUZ ORIVE, L.-M. 1976. Particle size-shape distributions: the general spheroid problem. I. Mathematical model. *J. Microsc. (Oxf.)*. **107**:235–253.
10. DELESSE, M. A. 1847. Procéde mécanique pour déterminer la composition des roches. *C. R. Acad. Sci.* **25**:544.

11. DULBECCO, R., and G. FREEMAN. 1959. Plaque production by the polyoma virus. *Virology*. **8**:396–397.
12. ENGLAND, J. M., and G. ATTARDI. 1974. Expression of the mitochondrial genome in HeLa cells. XXI. Mitochondrial protein synthesis during the cell cycle. *J. Mol. Biol.* **85**:433–444.
13. FARQUHAR, M. G., and G. E. PALADE. 1965. Cell junctions in amphibian skin. *J. Cell Biol.* **26**:263–291.
14. FRANKLIN, J. N. 1977. Some stereological principles in morphometric cytology. *SIAM (Soc. Ind. Appl. Math.) J. Appl. Math. Part C*. In press.
15. GRIMES, G. W., H. R. MAHLER, and P. S. PERLMAN. 1974. Nuclear gene dosage effects on mitochondrial mass and DNA. *J. Cell Biol.* **61**:565–574.
16. HAMMERSLEY, J., and D. HANDSCOMB. 1964. *Monte Carlo Methods*. John Wiley & Sons, Inc., New York.
17. HAWLEY, E. S., and R. P. WAGNER. 1967. Synchronous mitochondrial division in *Neurospora crassa*. *J. Cell Biol.* **35**:489–499.
18. JACOB, F., S. BRENNER, and F. CUZIN. 1963. On the regulation of DNA replication in bacteria. *Cold Spring Harbor Symp. Quant. Biol.* **28**:329–348.
19. KOLB-BACHOFEN, V., and W. VOGELL. 1975. Mitochondrial proliferation in synchronized cells of *Tetrahymena pyriformis*. *Exp. Cell Res.* **94**:95–105.
20. KROON, A. M., and C. SACCONE, editors. 1974. *The Biogenesis of Mitochondria*. Academic Press, Inc., New York.
21. LINNANE, A. W., and J. M. HASLAM. 1970. The biogenesis of yeast mitochondria. *Curr. Top. Cell. Regul.* **2**:101–172.
22. LITTLE, D. V. 1974. A third note on recent research in geometrical probability. *Adv. Appl. Probab.* **6**:103–130.
23. LUCK, D. J. L. 1963. Genesis of mitochondria in *Neurospora crassa*. *Proc. Natl. Acad. Sci. U. S. A.* **49**:233–240.
24. LUCK, D. J. L. 1963. Formation of mitochondria in *Neurospora crassa*. A quantitative radioautographic study. *J. Cell Biol.* **16**:483–499.
25. LUCK, D. J. L. 1965. Formation of mitochondria in *Neurospora crassa*. A study based on mitochondrial density changes. *J. Cell Biol.* **24**:461–470.
26. MAYHEW, T. M., and L.-M. CRUZ. 1973. Stereological correction procedures for estimating true volume proportions from biased samples. *J. Microsc. (Oxf.)*. **99**:287–299.
27. MAYHEW, T. M., and L.-M. CRUZ ORIVE. 1974. Caveat on the use of the Delesse principle of areal analysis for estimating component volume densities. *J. Microsc. (Oxf.)*. **102**:195–207.
28. MITCHISON, J. M. 1971. *The Biology of the Cell Cycle*. Cambridge University Press, Cambridge.
29. MORAN, P. A. P. 1966. A note on recent research in geometrical probability. *J. Appl. Probab.* **3**:453–463.
30. MORAN, P. A. P. 1969. A second note on recent research in geometrical probability. *Adv. Appl. Probab.* **1**:73–89.
31. OSUMI, M., and N. SANDO. 1969. Division of yeast mitochondria in synchronous culture. *J. Electron Microsc.* **18**:47–56.
32. PARSONS, J. A., and R. C. RUSTAD. 1968. The distribution of DNA among dividing mitochondria of *Tetrahymena pyriformis*. *J. Cell Biol.* **37**:683–693.
33. PICA-MATTOCIA, L., and G. ATTARDI. 1971. Expression of the mitochondrial genome in HeLa cells. V. Transcription of mitochondrial DNA in relationship to the cell cycle. *J. Mol. Biol.* **57**:615–621.
34. PICA-MATTOCCIA, L., and G. ATTARDI. 1972. Expression of the mitochondrial genome in HeLa cells. IX. Replication of mitochondrial DNA in relationship to the cell cycle in HeLa cells. *J. Mol. Biol.* **64**:465–484.
35. POSAKONY, J. W., J. M. ENGLAND, and G. ATTARDI. 1975. Morphological heterogeneity of HeLa cell mitochondria visualized by a modified diaminobenzidine staining technique. *J. Cell Sci.* **19**:315–329.
36. ROBBINS, E., and P. I. MARCUS. 1964. Mitotically synchronized mammalian cells: a simple method for obtaining large populations. *Science (Wash. D. C.)*. **144**:1152–1153.
37. ROSS, D. W., and H. C. MEL. 1972. Growth dynamics of mitochondria in synchronized Chinese hamster cells. *Biophys. J.* **12**:1562–1572.
38. SCHATZ, G., and T. L. MASON. 1974. The biosynthesis of mitochondrial proteins. *Annu. Rev. Biochem.* **43**:51–87.
39. SIANO, D. B. 1972. The log-normal distribution function. *J. Chem. Educ.* **49**:755–757.
40. SINCLAIR, W. K., and D. W. ROSS. 1969. Modes of growth in mammalian cells. *Biophys. J.* **9**:1056–1070.
41. STORRIE, B., and G. ATTARDI. 1973. Mode of mitochondrial formation in HeLa cells. *J. Cell Biol.* **56**:833–838.
42. TANDLER, B., R. A. ERLANDSON, S. L. SMITH, and E. L. WYNDER. 1969. Riboflavin and mouse hepatic cell structure and function. II. Division of mitochondria during recovery from simple deficiency. *J. Cell Biol.* **41**:477–493.
43. TANDLER, B., and C. L. HOPPEL. 1973. Division of giant mitochondria during recovery from cuprizone intoxication. *J. Cell Biol.* **56**:266–272.
44. TERASIMA, T., and L. S. TOLMACH. 1963. Growth and nucleic acid synthesis in synchronously dividing populations of HeLa cells. *Exp. Cell Res.* **30**:344–362.
45. THOMAS, G. B., JR. 1968. *Calculus and Analytic Geometry*. Addison-Wesley Publishing Co., Reading, Mass.
46. VENABLE, J. H., and R. COGGESHALL. 1965. A

simplified lead citrate stain for use in electron microscopy. *J. Cell Biol.* **25:**407–408.

47. WEIBEL, E. 1969. Stereological principles for morphometry in electron microscopic cytology. *Int. Rev. Cytol.* **26:**235–302.
48. WEIBEL, E., and D. M. GOMEZ. 1962. A principle for counting tissue structures on random sections. *J. Appl. Physiol.* **17:**343–348.
49. WEIBEL, E., G. S. KISTLER, and W. F. SCHERLE. 1966. Practical stereological methods for morphometric cytology. *J. Cell Biol.* **30:**23–38.
50. YUAN, P.-T. 1933. On the logarithmic frequency distribution and the semi-logarithmic correlation surface. *Ann. Math. Stat.* **4:**30–74.